

# Estimating the Membrane Properties of Vestibular Type II Hair Cells using Continuous-time System Identification <sup>\*</sup>

Siqi Pan<sup>\*</sup> James S. Welsh<sup>\*</sup> Alan M. Brichta<sup>\*\*</sup>  
Hannah R. Drury<sup>\*\*</sup> Jeremy G. Stoddard<sup>\*</sup>

<sup>\*</sup> School of Electrical Engineering and Computing, University of Newcastle, Australia (e-mails: siqi.pan@uon.edu.au, james.welsh@newcastle.edu.au, jeremy.stoddard@uon.edu.au)

<sup>\*\*</sup> School of Biomedical Sciences and Pharmacy, University of Newcastle, Australia (e-mails: alan.brichta@newcastle.edu.au, hannah.drury@newcastle.edu.au)

---

**Abstract:** In this paper we apply a continuous-time system identification method, known as the Simplified Refined Instrumental Variable method for Continuous-time systems (SRIVC), to the problem of estimating membrane properties of vestibular Type II hair cells. Due to the non-ideal characteristics of the experimental system, additional parameters, other than those of the membrane are required to be estimated. The SRIVC algorithm is modified to allow known poles and zeros to be forced into the estimator. This modified algorithm is then applied to the identification of the membrane properties of vestibular Type II hair cells, yielding results commensurate with typically accepted values.

*Keywords:* System identification, Continuous-time systems, Instrumental variable method, Biological systems

---

## 1. INTRODUCTION

Measurements of the membrane properties of cells can provide useful information on intrinsic processes occurring within the cell. For example, alteration of membrane capacitance during cell depolarisation provides insights into intrinsic cellular events such as ‘exocytosis’, a process in neurons where packets of internally stored neurotransmitter are released from the cell body into the external medium (Joshi and Fernandez, 1988). Numerous complexities arise in quantifying the membrane properties, including a requirement for precise experimental conditions to record the small electrical signals from a cell and a suitable estimation method to compute the membrane parameters.

Single electrode whole-cell voltage-clamp recording is a ‘patch-clamp’ technique that has been in use since the 1980’s (Hamill et al., 1981) to acquire small, high resolution, low noise electrical signals from excitable cells. In voltage-clamp recordings, the membrane potential is held constant or ‘clamped’, while the current that flows through the membrane is measured. The membrane current provides a measure of membrane conductance, which is directly proportional to the activity of voltage-gated ion channels (Sakmann and Neher, 1984). The single electrode whole-cell voltage-clamp technique uses a glass micropipette for both voltage and current recordings. A blunt micropipette is used to make a tight seal with the membrane. The patch of membrane directly under the pipette orifice is subsequently ruptured with a brief pulse

of negative pressure so that the micropipette provides a low-resistance access to the whole cell, hence the term whole-cell patch-clamp technique (Molnar and Hickman, 2007). Three parameters of interest are measured, namely the membrane capacitance,  $C_m$ , the membrane resistance,  $R_m$ , and the series resistance,  $R_s$ . The first two parameters allow us to monitor changing cell conditions, and the third provides a measure of the patency and integrity of the patch. Monitoring these parameters allows us to determine the time course and duration of changes in cell membrane properties.

Typically, to estimate membrane properties, curve-fitting techniques are applied to find the time constant of the current response to a voltage step (Maertz, 2012). The membrane capacitance can then be estimated based on a simple admittance model of the hair cell. Single-frequency admittance analysis has also been used to estimate the change in membrane capacitance by detecting the change in phase angle of the current output (Gillis, 1995). The real and imaginary parts of the admittance at a particular frequency as well as a DC component are used to estimate  $C_m$ ,  $R_m$  and  $R_s$ . A more sophisticated approach is the multi-frequency analysis, which allows simultaneous estimates of  $C_m$ ,  $R_m$  and  $R_s$  (Joshi and Fernandez, 1988; Santos-Sacchi, 2004; Farrell et al., 2006) and is less prone to noise that affects the single-frequency approach. We note that the above approaches do not, in general, take into consideration the effect of parasitic components and the filtering actions inherent in the experimental setup.

In this paper, we apply continuous-time (CT) system identification to estimate the membrane parameters of

---

<sup>\*</sup> This work was supported by the Australian government Research Training Program (RTP) scholarship

vestibular Type II hair cells in mice aged between 3 and 6 weeks. One of the advantages of identifying a CT model from sampled data is that the transfer function coefficients are directly linked to physical parameters, which allows the hair cell parameters to be readily computed. It is known that stray capacitance exists between all conducting elements of the recording equipment, in the order of a few picofarads (Maertz, 2012), that may have a significant effect on the estimated parameters if not taken into consideration. The majority of the stray capacitance exists between the micropipette and ground as well as at the terminal of the headstage amplifier and ground. In this paper, it is found that the stray capacitance has a significant impact on the system dynamics in the frequency range of interest. Instead of directly using the well-established first order admittance model of the hair cell in the literature, which only includes the  $C_m$ ,  $R_m$  and  $R_s$  parameters, we also consider the additional stray capacitance due to the recording equipment as part of the model. This new model structure requires a modification to the CT identification method due to the issue arising from its relative degree.

The remainder of the paper is organised as follows. Section 2 outlines the experimental setup, the equivalent circuit of the hair cell and the problem statement. Section 3 provides system and model definitions as well as a description of the SRIVC estimator and its modified version. The identification results are presented in Section 4, and the paper is concluded in Section 5.

## 2. PRELIMINARIES AND PROBLEM STATEMENT

This section describes the experimental setup of the in vitro patch-clamp recording, followed by an explanation on the equivalent circuit of the hair cell and a statement on the identification problem.

### 2.1 Experimental Setup

The setup of the patch-clamp recording is shown in Fig. 1. A command input from the personal computer (PC) is converted to an analog signal and passed through the Axopatch 1D amplifier (Molecular Devices, Sunnyvale, USA). This signal then goes through the headstage amplifier, which has an electrode enclosed in a glass micropipette attached to its terminal, to stimulate and record from the cell. The input voltage received by the cell is also monitored by the Axopatch 1D amplifier and sent to the PC. This is known as the monitor input voltage. The headstage amplifier consists of a current-to-voltage converter and some scaling circuitry, i.e. the voltage output from the headstage amplifier corresponds to the measured membrane current (Maertz, 2012). The measured output passes through an analog 10 kHz anti-aliasing Bessel filter before being converted to a digital signal and sent back to the PC. The monitor voltage and measured current were used as the input and output signals respectively in the identification procedure to estimate the cell parameters.

### 2.2 Equivalent Circuit of a Hair Cell

A cell acquires its electrical properties from its membrane, which consists of a double lipid layer that separates ions from the interior and the exterior of the cell (Maertz, 2012). This allows the cell membrane to maintain a potential difference, created by the pumping of sodium and

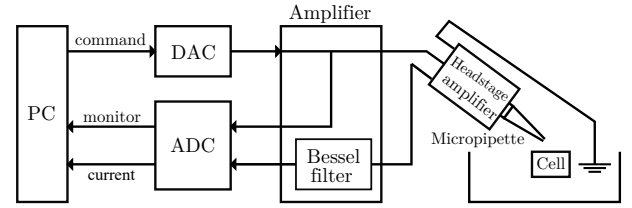


Fig. 1. Experimental setup of the patch-clamp recording of the hair cell.

potassium ions. In addition to ionic pumps, voltage-gated ion channels in the membrane can open and allow current to flow and hence membrane conductance increases. Furthermore, the cell membrane can also be viewed as an insulator separating opposing charges, which means the membrane also possesses capacitance. Since capacitance is proportional to the area of the conducting surface, membrane capacitance increases with cell size. Hence, a cell membrane can be modeled as a resistor,  $R_m$ , in parallel with a capacitor,  $C_m$  (Maertz, 2012). During a whole-cell patch-clamp recording, a glass micropipette is sealed onto the surface of the membrane by an abrupt negative pressure applied to the cell. An electrolyte solution in the micropipette then forms an electrical continuity with the interior of the cell (Maertz, 2012). This adds a resistance,  $R_s$ , in series with the “equivalent” circuit of the cell membrane. There are stray capacitances associated with the output terminal of the headstage amplifier,  $C_h$ , as well as due to the electrode in the micropipette,  $C_p$ . The overall effect of stray capacitance is modeled by  $C_s$ . The equivalent circuit of a hair cell during a patch-clamp recording is shown in Fig. 2.

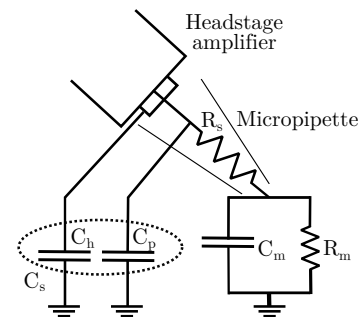


Fig. 2. Equivalent circuit of the hair cell during patch-clamp recordings.

The admittance model of the circuit in Fig. 2 is given by

$$M(s) = \frac{I(s)}{V(s)} = \frac{b_0 s^2 + b_1 s + b_2}{s + a_1}, \quad (1)$$

where

$$b_0 = C_s, \quad b_1 = \frac{R_m C_m + R_s C_s + R_m C_s}{R_m R_s C_m} \quad (2)$$

$$b_2 = \frac{1}{R_m R_s C_m}, \quad a_1 = \frac{R_m + R_s}{R_m R_s C_m}.$$

Notice the relative degree of -1 of the admittance model in (2). In an exact circuit representation, there would be an extremely small conductance in parallel with the stray capacitance, which would make the model proper. However, the dynamics associated with the conductance does not affect the system response in the frequency region of interest, hence is not included in the model.

### 2.3 Problem Statement

All the cell experiments presented in this paper have a 10 kHz analog anti-aliasing Bessel filter applied to the measured output. The coefficients of this analog Bessel filter are identified first since they are not known exactly. The effect of this filter is then taken into consideration by applying it to the measured input as the dynamics of the filter are close in frequency to the dynamics of the cells under study. A problem associated with the hair cell identification is that the admittance model has a relative degree of -1. This improper transfer function cannot be easily simulated in the standard SRIVC algorithm, which uses the `lsim` command in MATLAB to produce the time-domain response of dynamic systems. Hence, the SRIVC algorithm is modified to handle this problem. Note that all identification procedures are conducted using input voltage in mV and the output current in nA.

### 2.4 Figure of Merit

A figure of merit based on the normalised fit (Ljung, 1999) is used as a measure of the validation accuracy of the estimated model:

$$R^2 = 1 - \left( \frac{1}{N} \sum_{t=1}^N (y_m(t_k) - y(t_k))^2 \right) / \left( \frac{1}{N} \sum_{t=1}^N y(t_k)^2 \right), \quad (3)$$

where  $y_m$  is the model output,  $y$  the output in the validation dataset and  $N$  the total number of samples. Note that  $R^2 = 1$  indicates a perfect fit.

## 3. OUTLINE OF THE CONTINUOUS-TIME IDENTIFICATION METHOD

In this section, we first provide the CT system and model definitions, and then briefly review the Simplified Refined Instrumental Variable method for Continuous-time systems (SRIVC). The SRIVC estimator was first developed in Young and Jakeman (1980) and has achieved remarkable success in many practical applications (Young, 2011; Garnier and Wang, 2008), with the consistency property of this estimator recently proven under mild conditions in Pan et al. (2020). Due to the structure of the admittance model having a relative degree of -1, a modified version of the SRIVC algorithm is provided for the identification of the hair cell membrane parameters.

### 3.1 CT System and Model Definitions

The CT system is given by

$$S: \begin{cases} \dot{\hat{x}}(t) &= \frac{B(p)}{A(p)} \hat{u}(t) \\ y(t) &= \hat{x}(t) + v(t), \end{cases}$$

where  $p$  is the differential operator,  $v(t) = H(p)e(t)$  with  $H(p)$  being a stable filter and  $e(t)$  a zero-mean Gaussian noise, i.e.  $e \sim N(0, \sigma^2)$ . The system polynomial with degrees  $n \geq m$  are defined as

$$\begin{aligned} B^*(p) &= b_0^* p^m + b_1^* p^{m-1} + \dots + b_m^*, \\ A^*(p) &= p^n + a_1^* p^{n-1} + \dots + a_n^*. \end{aligned}$$

Since only sampled input-output data are available as measurements, the output observation equation of the CT system at the sample instant,  $t_k$ , becomes

$$y(t_k) = \hat{x}(t_k) + v(t_k). \quad (4)$$

Due to the difficulty of dealing with the time-derivatives of stochastic noise, which does not have a finite variance, and the discrete-time nature of the sampled signals, we only consider discrete-time noise as in (4) in this paper.

We then assume the model order is known exactly, and the CT model is therefore parameterised as

$$M: \begin{cases} x(t_k) &= \frac{B(p)}{A(p)} u(t_k) \\ y(t_k) &= x(t_k) + \varepsilon(t_k), \end{cases} \quad (5)$$

where

$$\begin{aligned} B(p) &= b_0 p^m + b_1 p^{m-1} + \dots + b_m \\ A(p) &= p^n + a_1 p^{n-1} + \dots + a_n, \end{aligned} \quad (6)$$

and the model parameters to be estimated are given by

$$\theta = [a_1 \dots a_n \ b_0 \dots b_m]^\top.$$

### 3.2 The SRIVC Estimator

The iterative SRIVC estimator minimises the sum of squares of the generalised equation error (GEE) (Young, 1981),  $\varepsilon(t_k)$ , which is defined as

$$\begin{aligned} \varepsilon(t_k) &= y(t_k) - \frac{B(p)}{A(p)} u(t_k) \\ &= A(p) \left\{ \frac{1}{A(p)} y(t_k) \right\} - B(p) \left\{ \frac{1}{A(p)} u(t_k) \right\}, \end{aligned} \quad (7)$$

Due to the iterative nature of the SRIVC method, the  $(j+1)$ -th iteration of the SRIVC estimate (Young and Jakeman, 1980), based on the parameter values estimated in the  $j$ -th iteration, is given by

$$\theta_{j+1} = \left[ \frac{1}{N} \sum_{k=1}^N \hat{\varphi}_f(t_k) \varphi_f^\top(t_k) \right]^{-1} \left[ \frac{1}{N} \sum_{k=1}^N \hat{\varphi}_f(t_k) y_f(t_k) \right], \quad (8)$$

where

$$\varphi_f(t_k) = \frac{1}{A_j(p)} \left[ -p^{n-1} y(t_k) \dots -y(t_k) \right. \\ \left. p^m u(t_k) \dots u(t_k) \right]^\top, \quad (9)$$

$$\hat{\varphi}_f(t_k) = \frac{1}{A_j(p)} \left[ -\frac{B_j(p)}{A_j(p)} p^{n-1} u(t_k) \dots -\frac{B_j(p)}{A_j(p)} u(t_k) \right. \\ \left. p^m u(t_k) \dots u(t_k) \right]^\top, \quad (10)$$

and

$$y_f(t_k) = \frac{p^n}{A_j(p)} y(t_k).$$

### 3.3 Modified SRIVC Estimator with a Forced Pole or Zero

The standard SRIVC estimator requires a proper transfer function model for simulation purposes. To avoid the problem of having an improper transfer function in (1), the measured output is filtered with a transfer function with a unity DC gain and a pole that is much faster than the dynamics of the system. This known pole is then forced into the SRIVC algorithm so that only the unknown parameters are estimated. To explain this procedure, consider the cell model  $M(p)$  in (1) with  $s$  replaced by the differential operator and a transfer function  $F(p)$  with a unity gain and a fast pole  $\alpha$ , i.e.

$$F(p) = \frac{\alpha}{p + \alpha}.$$

The combined transfer function is therefore

$$\tilde{M}(p) = M(p)F(p) = \frac{\alpha(b_0p^2 + b_1p + b_2)}{p^2 + (\alpha + a_1)p + \alpha a_1}.$$

Substituting the numerator and denominator polynomials of  $\tilde{M}(p)$  into (7), we can express the GEE as

$$\begin{aligned} \tilde{\varepsilon}(t_k) &= (p^2 + \alpha p + a_1 p + a_1 \alpha) y_f(t_k) \\ &\quad - (b_0 \alpha p^2 + b_1 \alpha p + b_2 \alpha) u_f(t_k) \\ &= y_f^{(2)}(t_k) + \alpha y_f^{(1)}(t_k) + a_1 (y_f^{(1)}(t_k) + \alpha y_f(t_k)) \\ &\quad - b_0 \alpha u_f^{(2)}(t_k) - b_1 \alpha u_f^{(1)}(t_k) - b_2 \alpha u_f(t_k), \end{aligned}$$

where  $u^{(i)}(t_k) = p^i u(t_k)$ . The pseudo-linear regression can then be written as

$$\tilde{y}_f(t_k) = \tilde{\varphi}_f^\top(t_k) \theta + \varepsilon(t_k),$$

where

$$\tilde{y}_f(t_k) = y_f^{(2)}(t_k) + \alpha y_f^{(1)}(t_k),$$

$$\tilde{\varphi}_f(t_k) = [-(y_f^{(1)}(t_k) + \alpha y_f(t_k)), \alpha u_f^{(2)}(t_k), \alpha u_f^{(1)}(t_k),$$

and

$$\theta = [a_1 \ b_0 \ b_1 \ b_2]^\top.$$

The instrument vector can be modified in the same form as (11) to produce  $\tilde{\varphi}_f(t_k)$ , and together with  $\tilde{\varphi}_f(t_k)$  and  $\tilde{y}_f(t_k)$ , can be substituted into (8) to solve for the unknown parameter  $\theta$ . A similar modification procedure can be defined when forcing a zero into the SRIVC algorithm.

#### 4. RESULTS OF IDENTIFICATION

In this section, the input signals used in the identification process are firstly introduced. This is followed by the parameter estimation results of the Bessel filter and two Type II vestibular hair cells.

##### 4.1 Experiment Inputs

Two types of inputs are used in the identification process, one for the identification of the Bessel filter, the other for the identification of the cell membrane parameters.

*Multisine* A multisine was used for identifying the Bessel filter, i.e.

$$u(t) = \sum_{i=1}^{10} \sin(2\pi f_i t + \phi_i), \quad (12)$$

where  $f = \{3, 6, 8, 10, 12, 14, 16, 29, 22, 24\}$  kHz and  $\phi_i = \phi_1 - \frac{i(i-1)\pi}{10}$ ;  $2 \leq i \leq 10$ .

*Square Waves* Two types of square waves, labelled S1 and S2, were used as the excitation signals for the hair cells. One cycle of the *S1 square wave* is shown in Fig. 3 (a) and two cycles of the *S2 square wave* are shown in Fig. 3 (b), where A is the amplitude of the signal and  $T_0$  is the inverse of the fundamental frequency of the input.

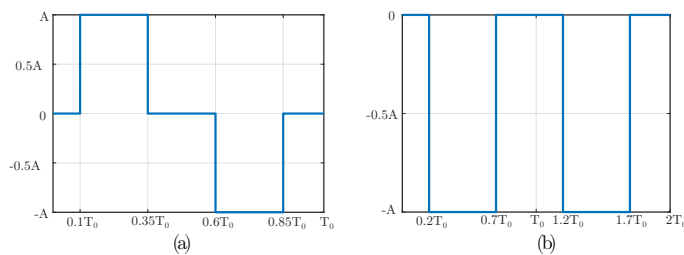


Fig. 3. S1 and S2 square wave inputs.

##### 4.2 Identification of the Bessel Filter

The multisine input in (12) was used as the excitation signal for the identification of the Bessel filter. The sampling frequency was 100 kHz, and the signal duration was 60 seconds. The first 50 seconds of data was used for estimation and the last 10 seconds for validation. A 9.1 M $\Omega$  resistor, denoted by  $R$ , was connected between the headstage amplifier and ground, then the input and output data were collected in order to identify the filter. A stray capacitance,  $C_s$ , in the range of 1.5 to 2 pF, is associated with the output terminal of the headstage amplifier. Some measurements performed on similar terminals showed that the stray capacitance was approximately 1.6 pF. This stray capacitance in parallel with the 9.1 M $\Omega$  resistor manifests itself as a zero in the 4th-order Bessel filter expression, which was forced into the modified SRIVC algorithm so that only the Bessel filter coefficients were estimated.

The 4th-order Bessel filter with a zero has the structure

$$F(s) = (b_3 s + b_4) F_{bessel}(s) = \frac{(b_3 s + b_4) a_4}{s^4 + a_1 s^3 + a_2 s^2 + a_3 s + a_4}, \quad (13)$$

where  $b_3 = C_s = 1.6 \times 10^{-6}$  and  $b_4 = 1/R = 1/9.1$ .

The relative magnitude of the filter coefficients in (13) are quite large due to its 4th order nature and large bandwidth. Hence, to avoid ill-conditioning of the normal matrix, time scaling was used to convert the filter coefficients to numbers with relatively similar magnitudes prior to identification. Let  $s = s' \omega_0$  and  $T'_s = T_s \omega_0$ , where  $s'$  and  $T'_s$  are the complex variable and sampling period after time scaling respectively. The scaling factor,  $\omega_0$ , was chosen to be 50000, which corresponded to  $T'_s = 0.5$  sec. This choice of  $\omega_0$  allowed the filter coefficients after scaling to be reasonably sized numbers. Now, the transfer function in (13) can be written as

$$\begin{aligned} F(s') &= \frac{(b_3 s' \omega_0 + b_4) a_4}{(s' \omega_0)^4 + a_1 (s' \omega_0)^3 + a_2 (s' \omega_0)^2 + a_3 (s' \omega_0) + a_4} \\ &= \frac{\left(\frac{b_3}{\omega_0^3} s' + \frac{b_4}{\omega_0^4}\right) a_4}{s'^4 + \frac{a_1}{\omega_0} s'^3 + \frac{a_2}{\omega_0^2} s'^2 + \frac{a_3}{\omega_0^3} s' + \frac{a_4}{\omega_0^4}} \\ &= \frac{(b_3 \omega_0 s' + b_4) a_4}{s'^4 + \alpha_1 s'^3 + \alpha_2 s'^2 + \alpha_3 s' + \alpha_4}, \end{aligned}$$

where  $\alpha_1 = \frac{a_1}{\omega_0}$ ,  $\alpha_2 = \frac{a_2}{\omega_0^2}$ ,  $\alpha_3 = \frac{a_3}{\omega_0^3}$  and  $\alpha_4 = \frac{a_4}{\omega_0^4}$ . Note that parameters  $b_3$  and  $b_4$  are forced into the modified SRIVC algorithm, and only  $\{\alpha_i\}_{i=1}^4$  are estimated and then convert to the original coefficients  $\{a_i\}_{i=1}^4$  in (13). The estimated Bessel filter coefficients are given in Table 1.

Table 1. Estimated Bessel filter coefficients.

$a_1$	$a_2$	$a_3$	$a_4$
$1.998 \times 10^5$	$2.635 \times 10^{10}$	$1.618 \times 10^{15}$	$4.930 \times 10^{19}$

The time and frequency domain plots for the Bessel filter are shown in Fig. 4 and Fig. 5 respectively. The predicted output matched well with the measurements in both domains. This good fit was then confirmed by the figure of merit (3), which was 0.9962 based on the validation data.

##### 4.3 Identification of the Membrane Properties of Type II Vestibular Hair Cells

The patch-clamp technique was used to record current signals in the membrane of vestibular Type II hair cells

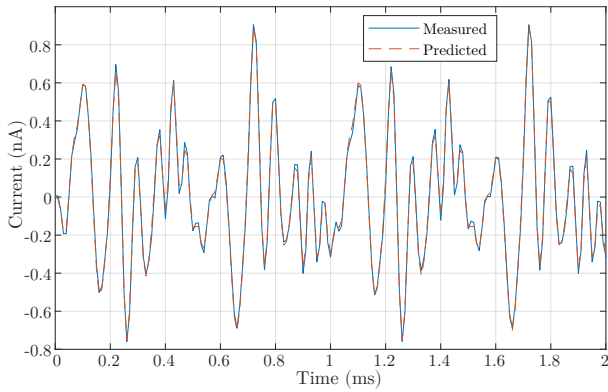


Fig. 4. Predicted vs. measured output for the Bessel filter estimation data in time domain.

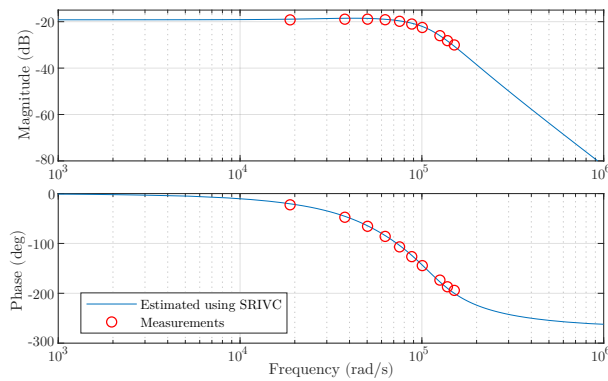


Fig. 5. Predicted vs. measured output for the Bessel filter estimation data in frequency domain.

in mice. Inputs were chosen to be square waves, which were superimposed with a DC offset of  $-60$  mV that corresponds to the resting membrane potential of the cell. This was to suppress the opening of voltage-gated channels of the membrane since the open channels would decrease the membrane resistance. The sampling frequency was  $100$  kHz, and the signal duration was  $10$  seconds. The first  $9$  seconds of data was used for estimation and the last second for validation. The identified Bessel filter, as specified in Table 1, was applied to the input prior to estimation to remove its effect from the system dynamics. The modified SRIVC algorithm in Section 3.3 was used with a fast pole of  $10^5$  rad/s to estimate the cell parameters. Voltage and current were recorded for two cells (labelled Cell 1 and 2). The experimental results of each cell are presented in chronological order to show signs (if any) of the deterioration of the cell and recording conditions. The nominal values for the typical Type II membrane parameters are:  $C_m = 4 - 8$  pF (Eatock and Lysakowski, 2006; Poppi et al., 2018; Moser and Beutner, 2000),  $R_m = 500$  M $\Omega - 1$  G $\Omega$  and  $R_s < 20$  M $\Omega$ . The parameter  $R_s$  is preferred to be kept below  $10$  M $\Omega$  during the experiment but can be tolerated up to  $20$  M $\Omega$ , above which the recordings become noisy.

*Estimation results of Cell 1* S1 square waves at  $5$ Hz,  $10$ Hz and  $50$ Hz (labelled Exp1, Exp2 and Exp3) with an amplitude of  $10$  mV and a  $-60$  mV DC offset were used as the excitation inputs for Cell 1. The identification results are summarised in Table 2.

Table 2. Summary of the Cell 1 results.

Input	$C_m$ (pF)	$R_m$ (M $\Omega$ )	$R_s$ (M $\Omega$ )	$C_s$ (pF)	$R_{val}^2$
Exp 1	6.52	530.90	6.49	5.60	0.9801
Exp 2	6.60	600.96	6.37	5.66	0.9896
Exp 3	6.64	704.49	6.42	5.72	0.9962

The  $C_m$  values were relatively constant as expected since the membrane capacitance was dependent on the size of the cell, which did not vary during the experiments. The  $R_s$  values were also constant and below  $10$  M $\Omega$ , indicating the glass micropipette maintained a good seal with good electrical access to the interior of the cell. As expected, the stray capacitance did not vary significantly. The time and frequency domain plots for Experiment 1 are shown in Fig. 6 and Fig. 7 respectively. By zooming in on the output, a slow rise in the steady state values could be observed occasionally, especially after an upward step in the input as shown in the lower right window of Fig. 6. This phenomenon was caused by the slow opening of some of the voltage-gated channels on the membrane. This may lead to an error in the  $R_m$  estimate since its value depends heavily on the DC gain of the system as shown in (2). This would explain the increase of  $R_m$  values from Experiments 1 to 3 as shown in Table 2. The  $5$  Hz square wave used in Experiment 1 had a longer duration at  $-50$  mV per cycle as compared to the  $50$  Hz input in Experiment 3, which means that the  $5$  Hz input would have allowed more channels to open, hence resulting in a lower  $R_m$  value. Therefore, to further minimise the channels opening, the voltage inputs were modified for the Cell 2 recordings.

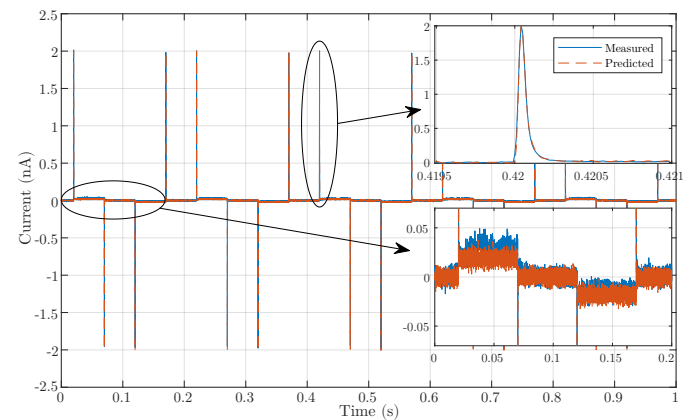


Fig. 6. Predicted vs. measured output for Cell 1 Experiment 1 estimation data in time domain.

*Estimation results of Cell 2* Instead of using a  $20$  mV peak-to-peak square wave centred around  $-60$  mV, the inputs of the four experiments for Cell 2 were kept between  $-70$  and  $-60$  mV to further minimise channels opening on the cell membrane. Experiments 1 and 3 used  $5$  Hz and  $10$  Hz S2 square waves with an amplitude of  $10$  mV and a DC offset of  $-60$  mV. Experiments 2 and 4 used  $5$  Hz and  $10$  Hz S1 square waves held at  $-65$  mV with an amplitude of  $5$  mV. The estimated parameters of Cell 2 are summarised in Table 3.

The values of  $C_m$ ,  $R_s$  and  $C_s$  for Cell 2 were relatively constant throughout the experiments. After reducing the likelihood of opening channels on the membrane,  $R_m$  was seen to be less variable across the experiments. This was

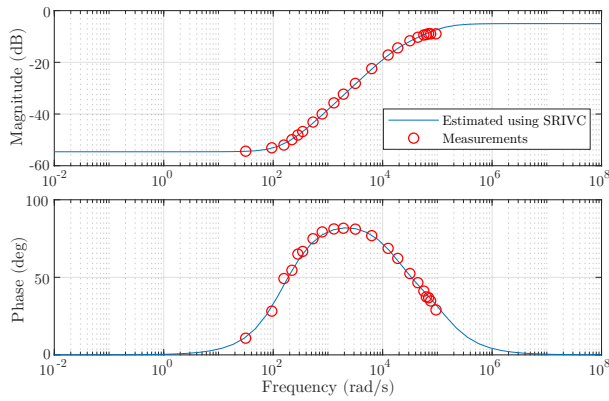


Fig. 7. Predicted vs. measured output for Cell 1 Experiment 1 estimation data in frequency domain.

Table 3. Summary of the Cell 2 results.

Input	$C_m$ (pF)	$R_m$ (M $\Omega$ )	$R_s$ (M $\Omega$ )	$C_s$ (pF)	$R^2_{total}$
Exp 1	7.47	748.92	10.68	6.22	0.9711
Exp 2	7.43	736.50	10.89	6.23	0.9556
Exp 3	7.40	733.58	10.67	6.35	0.9862
Exp 4	7.46	712.36	10.34	6.31	0.9725

confirmed by the constant steady state measured output as shown in the bottom right window in Fig. 8. The membrane capacitance was approximately 7.4 pF, which meant Cell 2 was slightly larger than Cell 1. A higher  $R_s$  value indicated that the electrical access between the micropipette and the cell was less than that of Cell 1. The  $C_s$  values were different as compared to those obtained with Cell 1, which was likely due to the electrode being positioned differently for the Cell 2 recordings and the level of fluid in the recording chamber being different.

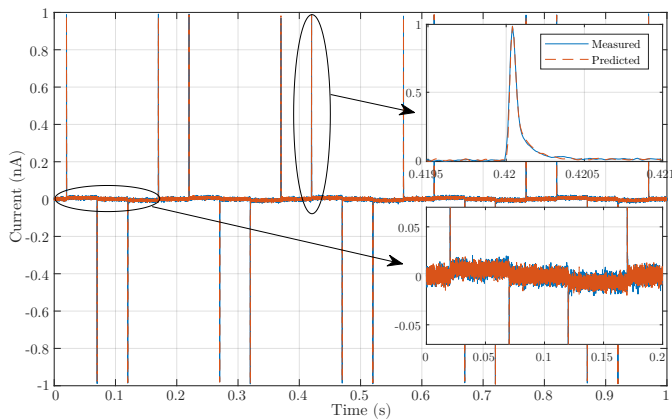


Fig. 8. Predicted vs. measured output for Cell 2 Experiment 2 estimation data in time domain.

## 5. CONCLUSION AND FUTURE WORK

In this paper, we have shown that the SRIVC estimator can be applied successfully to the identification of the membrane properties of Type II vestibular hair cells of mice. The standard SRIVC algorithm was modified to allow known poles/zeros to be forced into the estimator. Using this approach, we were able to estimate the membrane parameters as well as the stray capacitance due to the recording instrument, which was also considered as part of the hair cell model. The figure of merit,  $R^2$ , used

in validation showed that the estimated model was highly accurate. It is envisaged that this methodology provides much greater accuracy than the existing membrane parameter estimation methods given that it explicitly considers the effect of stray capacitance and the anti-aliasing filter.

## REFERENCES

- Eatock, R.A. and Lysakowski, A. (2006). *Vertebrate Hair Cells*, chapter Mammalian Vestibular Hair cells, 348 – 442. Springer.
- Farrell, B., Shope, C.D., and Brownel, W.E. (2006). Voltage-dependent capacitance of human embryonic kidney cells. *Phys Rev E Stat Nonlin Soft Matter Phys*, 73(4), 041930.
- Garnier, H. and Wang, L. (eds.) (2008). *Identification of Continuous-time Models from Sampled data*. Springer.
- Gillis, K.D. (1995). Techniques for membrane capacitance measurements. *Single-Channel Recording*, 155 – 198.
- Hamill, O.P., Neher, M.E., Sakmann, B., and Sigworth, F.J. (1981). Improved patch-clamp techniques for high-resolution current recording from cells and cell-free membrane patches. *European Journal of Physiology*, 391, 85 – 100.
- Joshi, C. and Fernandez, J.M. (1988). Capacitance measurements: An analysis of the phase detector technique used to study exocytosis. *Biophysical Society*, 885 – 892.
- Ljung, L. (1999). *System identification: Theory for the user*. Prentice Hall.
- Maertz, W.H. (2012). *The Axon Guide: A guide to Electrophysiology and Biophysics Laboratory Techniques*. Molecular Devices.
- Molnar, P. and Hickman, J.J. (2007). *Patch-Clamp Methods and Protocols*. Humana Press Inc., Totowa, New Jersey.
- Moser, T. and Beutner, D. (2000). Kinetics of exocytosis and endocytosis at the cochlear inner hair cell afferent synapse of the mouse. *Proceedings of the National Academy of Sciences*, 97(1), 883 – 888.
- Pan, S., González, R.A., Welsh, J.S., and Rojas, C.R. (2020). Consistency analysis of the simplified refined instrumental variable method for continuous-time systems. *Automatica*, 113.
- Poppi, L.A., Tabatabaee, H., Drury, H.R., Jobling, P., Callister, R.J., Migliaccio, A.A., Jordan, P.M., Holt, J.C., Rabbitt, R.D., Lim, R., and Brichta, A.M. (2018). Ach-induced hyperpolarization and decreased resistance in mammalian Type II vestibular hair cells. *J Neurophysiol*, 119(1), 312 – 325.
- Sakmann, B. and Neher, E. (1984). Patch clamp techniques for studying ionic channels in excitable membranes. *Annu Rev Physiol*, 46, 455 – 472.
- Santos-Sacchi, J. (2004). Determination of cell capacitance using the exact empirical solution of  $\partial Y/\partial C_m$  and its phase angle. *Biophysical Journal*, 87, 714 – 727.
- Young, P.C. (1981). Parameter estimation for continuous-time models – a survey. *Automatica*, 17(1), 23–39.
- Young, P.C. (2011). *Recursive estimation and time-series analysis: An introduction for the student and practitioner*. Springer-Verlag.
- Young, P.C. and Jakeman, A.J. (1980). Refined instrumental variable methods of recursive time-series analysis part III. Extensions. *International Journal of Control*, 31(4), 741–764.